

$\mathcal{O}(\alpha)$ electroweak corrections to the processes $e^+e^- \rightarrow \tau^-\tau^+, c\bar{c}, b\bar{b}, t\bar{t}$ – a comparison –*

T. HAHN^{a†}, W. HOLLIK^a,
A. LORCA^b, T. RIEMANN^b, AND A. WERTHENBACH^c

^a*Max-Planck-Institut für Physik, Föhringer Ring 6, D-80805 Munich, Germany*

^b*DESY Zeuthen, Platanenallee 6, D-15738 Zeuthen, Germany*

^c*CERN, TH Division, CH-1211 Genève 23, Switzerland*

Abstract

We present the electroweak one-loop corrections to the processes $e^+e^- \rightarrow f\bar{f}$, $f = \tau, c, b, t$, at energies relevant for a future linear collider. The results of two independent calculations are compared and agreement is found at a technical-precision level of ten to twelve digits.

1 Introduction

With the advent of the next linear collider (LC), center-of-mass energies will rise up to several hundred GeV and the envisioned luminosity will be as high as 300 fb^{-1} . Evidently, a new era of precision physics is approaching. The experimental precision which can be achieved at such a machine will by far exceed all current standards and will be a challenge to experimentalists and theoreticians alike. To obtain reliable predictions for the next generation of linear colliders, the inclusion of electroweak one-loop corrections becomes essential.

Two-fermion production processes, such as

$$e^+e^- \rightarrow f\bar{f}(\gamma), \quad (1)$$

*Work supported in part by the European Community's Human Potential Programme under contract HPRN-CT-2000-00149 "Physics at Colliders" and by Sonderforschungsbereich/Transregio 9 of DFG "Computergestützte Theoretische Teilchenphysik." This research has also been supported by a Marie Curie Fellowship of the European Community's Research Training Project under contract HPMF-CT-2002-01694.

†E-mails: alejandro.lorca@desy.de, tord.riemann@desy.de, anja.werthenbach@cern.ch,
hahn@mppmu.mpg.de, hollik@mppmu.mpg.de.

play a leading role at typical LC energies as foreseen by [1]. In the late seventies the one-loop correction to muon-pair production was calculated for the first time [2], where the muons were considered to be massless. Ever since, fermion-pair production processes attracted attention and various masses were successively introduced into the calculation. Recently, a high degree of computational precision was achieved in numerically comparing various results on radiative corrections to top-pair production (see [3, 4] and references therein). Such comparisons are invaluable to ensure the establishment of reliable, well-tested codes.

Here, we extend the study [3] to other final states. In this particular comparison we do not include hard bremsstrahlung. This issue has been discussed in detail in [4, 5] and will be calculated for realistic applications by dedicated Monte-Carlo programs for 2- to 6-fermion production [6, 7, 8].

2 Cross-section formulae

2.1 Notation and conventions

In this section, we will outline the framework to compute electroweak corrections to differential and total cross-sections in $\mathcal{O}(\alpha)$ of the electromagnetic coupling. This includes one-loop amplitudes as well as soft-photon bremsstrahlung.

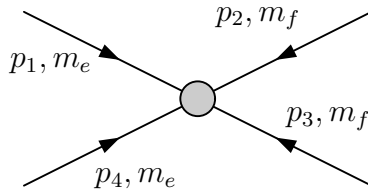


Figure 1: Definitions of the kinematical variables.

In a $2 \rightarrow 2$ -particle process we follow the momenta and mass convention of Fig. 1:

$$\frac{d\sigma}{d\cos\theta} = \frac{1}{32\pi} \frac{\beta_f}{s\beta_e} \sum_{\text{conf}} |\mathcal{M}_{ef}|^2, \quad (2)$$

where θ is the scattering angle. Furthermore we have

$$\beta_i \equiv \sqrt{1 - 4\frac{m_i^2}{s}} \quad (3)$$

$$s \equiv (p_1 + p_4)^2 = E_{\text{CM}}^2 \quad (4)$$

$$t \equiv (p_1 + p_2)^2 = -\frac{s}{2}(1 - \beta_e\beta_f \cos\theta) + m_e^2 + m_f^2 \quad (5)$$

$$u \equiv (p_1 + p_3)^2 = -\frac{s}{2}(1 + \beta_e\beta_f \cos\theta) + m_e^2 + m_f^2. \quad (6)$$

2.2 Unpolarized cross-section

We consider only the unpolarized cross-section and thus have to average over initial spin configurations (σ_e), sum over the final ones (σ_f), and add incoherently the number of colours (C_f) which cannot be distinguished:

$$\sum_{\text{conf}} |\mathcal{M}_{ef}|^2 = \frac{1}{4} \sum_{\sigma_e=1}^4 \sum_{\sigma_f=1}^4 C_f |\mathcal{M}_{ef}|^2. \quad (7)$$

The invariant transition amplitude \mathcal{M}_{ef} can be expressed in terms of a standard basis of matrix elements M_i , containing all the kinematical information of the interaction, and the form factors F_i , which account for the pure dynamical part:

$$\mathcal{M}_{ef} = \sum_i M_i F_i. \quad (8)$$

2.3 Neglecting the electron mass

In this comparative study we are neglecting the electron mass m_e in the purely weak contributions at the diagrammatic level, i.e. we neglect diagrams containing the electron–Higgs Yukawa coupling, which is proportional to the electron mass. This simplifies the final expression significantly and minimizes the number of independent form factors. We do not neglect the electron mass elsewhere so as to safely compute the photonic corrections.

2.4 Structure of $\mathcal{O}(\alpha)$ corrections

The hierarchy of contributions in the perturbative expansion of the $2 \rightarrow 2$ cross-section reads

$$\begin{aligned} |\mathcal{M}|^2 &= |\mathcal{M}_{ef}^{(0)} + \mathcal{M}_{ef}^{(1)} + \dots|^2 + |\mathcal{M}_\gamma^{(0)} + \dots|^2 \\ &= \underbrace{\mathcal{M}_{ef}^{(0)*} \mathcal{M}_{ef}^{(0)}}_{\mathcal{O}(\alpha^2)} + \underbrace{2 \operatorname{Re} \left(\mathcal{M}_{ef}^{(0)*} \mathcal{M}_{ef}^{(1)} \right)}_{\mathcal{O}(\alpha^3)} + \underbrace{\mathcal{M}_\gamma^{(0)*} \mathcal{M}_\gamma^{(0)}}_{\mathcal{O}(\alpha^4)} + \dots \end{aligned} \quad (9)$$

Soft-photon contributions are added to remove the infrared singularities of the photonic self-energies, vertices, and boxes.

For the Born amplitude, an appropriate basis for the matrix elements is:

$$\begin{aligned} M_1 &\equiv \bar{v}_e(p_4, \sigma_{e+}) \gamma^\mu \mathbb{1} \quad u_e(p_1, \sigma_{e-}) \otimes \bar{u}_f(-p_2, \sigma_f) \quad \gamma_\mu \mathbb{1} \quad v_f(-p_3, \sigma_{\bar{f}}) \\ M_2 &\equiv \bar{v}_e(p_4, \sigma_{e+}) \gamma^\mu \mathbb{1} \quad u_e(p_1, \sigma_{e-}) \otimes \bar{u}_f(-p_2, \sigma_f) \quad \gamma_\mu \gamma_5 \quad v_f(-p_3, \sigma_{\bar{f}}) \\ M_3 &\equiv \bar{v}_e(p_4, \sigma_{e+}) \gamma^\mu \gamma_5 \quad u_e(p_1, \sigma_{e-}) \otimes \bar{u}_f(-p_2, \sigma_f) \quad \gamma_\mu \mathbb{1} \quad v_f(-p_3, \sigma_{\bar{f}}) \\ M_4 &\equiv \bar{v}_e(p_4, \sigma_{e+}) \gamma^\mu \gamma_5 \quad u_e(p_1, \sigma_{e-}) \otimes \bar{u}_f(-p_2, \sigma_f) \quad \gamma_\mu \gamma_5 \quad v_f(-p_3, \sigma_{\bar{f}}). \end{aligned} \quad (10)$$

The differential Born cross-section finally reads

$$\left. \frac{d\sigma}{d \cos \theta} \right|_{\text{Born}} = \frac{1}{32\pi} \frac{\beta_f}{\beta_e} C_f \left\{ s(1 + \beta_e^2 \beta_f^2 \cos^2 \theta) \left(|F_1^{(0)}|^2 + |F_2^{(0)}|^2 + |F_3^{(0)}|^2 + |F_4^{(0)}|^2 \right) \right.$$

$$\begin{aligned}
& + 2s\beta_e\beta_f \cos\theta \left(F_1^{(0)*} F_4^{(0)} + F_2^{(0)*} F_3^{(0)} + F_3^{(0)*} F_2^{(0)} + F_4^{(0)*} F_1^{(0)} \right) \\
& + 4(m_f^2 + m_e^2) \left(|F_1^{(0)}|^2 - |F_4^{(0)}|^2 \right) + 4(m_f^2 - m_e^2) \left(-|F_2^{(0)}|^2 + |F_3^{(0)}|^2 \right) \\
& + 16 \frac{m_f^2 m_e^2}{s} \left(-|F_2^{(0)}|^2 - |F_3^{(0)}|^2 + 2|F_4^{(0)}|^2 \right) \Big\}, \tag{11}
\end{aligned}$$

with the form factors

$$F_1^{(0)} = ie^2 \left(+ V_e V_f \frac{1}{s - M_Z^2 + iM_Z \Gamma_Z} + Q_e Q_f \frac{1}{s} \right) \tag{12}$$

$$F_2^{(0)} = ie^2 \left(- V_e A_f \frac{1}{s - M_Z^2 + iM_Z \Gamma_Z} \right) \tag{13}$$

$$F_3^{(0)} = ie^2 \left(- A_e V_f \frac{1}{s - M_Z^2 + iM_Z \Gamma_Z} \right) \tag{14}$$

$$F_4^{(0)} = ie^2 \left(+ A_e A_f \frac{1}{s - M_Z^2 + iM_Z \Gamma_Z} \right). \tag{15}$$

The one-loop calculations for the different fermion flavours are very similar: Only the W–W-box diagram is different for different values of the isospin of the final-state fermion (see Fig. 2). These weak box diagrams were suppressed in applications to LEP1 physics but started to become numerically important at LEP2. They were studied systematically e.g. in Section 2.2 of [9] and Section 5.4 of [10], but a comparison with the published numbers is not straightforward.

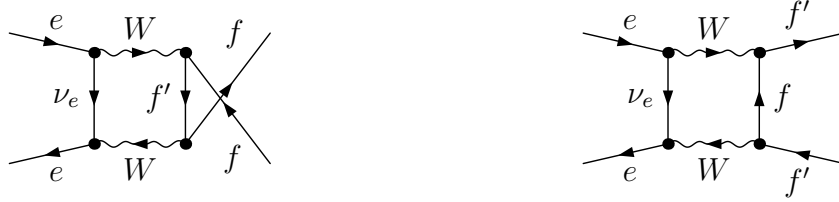


Figure 2: Electroweak W–W-box diagrams at the one-loop level, where f denotes an isospin-up and f' an isospin-down fermion.

At the one-loop level, with the appearance of vertex and box diagrams, the Lorentz structure of the matrix element is enriched:

$$\begin{aligned}
M_{1,k} &= \bar{v}_e(p_4, \sigma_{e+}) \gamma^\mu \{ \mathbb{1}, \gamma_5 \} u_e(p_1, \sigma_{e-}) \otimes \bar{u}_f(-p_2, \sigma_f) \gamma_\mu \{ \mathbb{1}, \gamma_5 \} v_f(-p_3, \sigma_{\bar{f}}) \\
M_{2,k} &= \bar{v}_e(p_4, \sigma_{e+}) \not{p}_2 \{ \mathbb{1}, \gamma_5 \} u_e(p_1, \sigma_{e-}) \otimes \bar{u}_f(-p_2, \sigma_f) \not{p}_4 \{ \mathbb{1}, \gamma_5 \} v_f(-p_3, \sigma_{\bar{f}}) \\
M_{3,k} &= \bar{v}_e(p_4, \sigma_{e+}) \not{p}_2 \{ \mathbb{1}, \gamma_5 \} u_e(p_1, \sigma_{e-}) \otimes \bar{u}_f(-p_2, \sigma_f) \{ \mathbb{1}, \gamma_5 \} v_f(-p_3, \sigma_{\bar{f}}) \\
M_{4,k} &= \bar{v}_e(p_4, \sigma_{e+}) \gamma^\mu \{ \mathbb{1}, \gamma_5 \} u_e(p_1, \sigma_{e-}) \otimes \bar{u}_f(-p_2, \sigma_f) \gamma_\mu \not{p}_4 \{ \mathbb{1}, \gamma_5 \} v_f(-p_3, \sigma_{\bar{f}}), \tag{16}
\end{aligned}$$

where the index k stands for the four possible combinations of $\{ \mathbb{1}, \gamma_5 \} \otimes \{ \mathbb{1}, \gamma_5 \}$ as in Eq. (10), leading to a basis of 16 elements. The one-loop contribution to the cross-section can be compacted in the following way:

$$\frac{d\sigma}{d\cos\theta} = \frac{d\sigma}{d\cos\theta} \Big|_{\text{Born}} + \frac{d\sigma}{d\cos\theta} \Big|_{1\text{-Loop}} \tag{17}$$

$$= \frac{d\sigma}{d \cos \theta} \Big|_{\text{Born}} + \frac{1}{32\pi} \frac{\beta_f}{\beta_e} C_f 2 \operatorname{Re} \left(\sum_{i=1}^4 F_i^{(0)*} \tilde{F}_i^{(1)} \right), \quad (18)$$

with form factors $\tilde{F}_i^{(1)}$ given by

$$\tilde{F}_i^{(1)} \equiv \frac{1}{s} \sum_{j,k=1}^4 M_{1,i}^\dagger M_{j,k} F_{j,k}^{(1)}, \quad (19)$$

that include the corresponding kinematical terms from the product of matrix elements¹ together with the one-loop form factors $F_{j,k}^{(1)}$, carefully defined in [5] and corresponding to the basis (16). The explicit expressions for these form factors $\tilde{F}_i^{(1)}$ are:

$$\begin{aligned} \tilde{F}_1^{(1)} &\equiv +4m_f^2 \left(F_{1,1}^{(1)} - F_{3,1}^{(1)} m_f \right) \\ &+ s \left\{ F_{1,1}^{(1)} + (F_{3,1}^{(1)} - 2F_{4,1}^{(1)} + 2F_{4,4}^{(1)}) m_f - F_{2,4}^{(1)} m_f^2 \right. \\ &\quad \left. + \beta_f \cos \theta \left(2F_{1,4}^{(1)} - F_{2,1}^{(1)} m_f^2 \right) + \beta_f^2 \cos^2 \theta \left(F_{1,1}^{(1)} - F_{3,1}^{(1)} m_f \right) \right\} \\ &+ \frac{s^2}{4} (1 - \beta_f^2 \cos^2 \theta) \left(F_{2,4}^{(1)} + \beta_f \cos \theta F_{2,1}^{(1)} \right) \end{aligned} \quad (20)$$

$$\begin{aligned} \tilde{F}_2^{(1)} &\equiv -4F_{1,2}^{(1)} m_f^2 \\ &+ s \left\{ F_{1,2}^{(1)} - F_{2,3}^{(1)} m_f^2 + \beta_f \cos \theta \left(2F_{1,3}^{(1)} + 2(F_{4,2}^{(1)} - F_{4,3}^{(1)}) m_f - F_{2,2}^{(1)} m_f^2 \right) \right. \\ &\quad \left. + \beta_f^2 \cos^2 \theta F_{1,2}^{(1)} \right\} + \frac{s^2}{4} (1 - \beta_f^2 \cos^2 \theta) \left(F_{2,3}^{(1)} + \beta_f \cos \theta F_{2,2}^{(1)} \right) \end{aligned} \quad (21)$$

$$\begin{aligned} \tilde{F}_3^{(1)} &\equiv +4m_f^2 \left(F_{1,3}^{(1)} - F_{3,3}^{(1)} m_f \right) \\ &+ s \left\{ F_{1,3}^{(1)} + (F_{3,3}^{(1)} + 2F_{4,2}^{(1)} - 2F_{4,3}^{(1)}) m_f - F_{2,2}^{(1)} m_f^2 \right. \\ &\quad \left. + \beta_f \cos \theta \left(+2F_{1,2}^{(1)} - F_{2,3}^{(1)} m_f^2 \right) + \beta_f^2 \cos^2 \theta \left(F_{1,3}^{(1)} - F_{3,3}^{(1)} m_f \right) \right\} \\ &+ \frac{s^2}{4} (1 - \beta_f^2 \cos^2 \theta) \left(F_{2,2}^{(1)} + \beta_f \cos \theta F_{2,3}^{(1)} \right) \end{aligned} \quad (22)$$

$$\begin{aligned} \tilde{F}_4^{(1)} &\equiv -4F_{1,4}^{(1)} m_f^2 \\ &+ s \left\{ F_{1,4}^{(1)} - F_{2,1}^{(1)} m_f^2 + \beta_f \cos \theta \left(2F_{1,1}^{(1)} + 2(-F_{4,1}^{(1)} + F_{4,4}^{(1)}) m_f - F_{2,4}^{(1)} m_f^2 \right) \right. \\ &\quad \left. + \beta_f^2 \cos^2 \theta F_{1,4}^{(1)} \right\} + \frac{s^2}{4} (1 - \beta_f^2 \cos^2 \theta) \left(F_{2,1}^{(1)} + \beta_f \cos \theta F_{2,4}^{(1)} \right). \end{aligned} \quad (23)$$

Many technical details of the underlying calculations have been described in [5, 11].

¹Since the corrections are of $\mathcal{O}(\alpha)$ with respect to the Born cross-section, we neglected the effect of the electron mass here.

3 Numerical results

In this section we present the numerical results for various final states at two typical LC energies: 500 GeV and 1 TeV. We performed two fixed-order calculations, i.e. no higher-order corrections such as photon exponentiation have been taken into account. The MPI Munich group performed a fully automated calculation using *FeynArts* [12, 13] and *FormCalc* [14], where the fermionic structures were evaluated in the Weyl–van-der-Waerden formalism [15] rather than by introducing helicity matrix elements $M_{j,k}$ as outlined before. The numbers of the Zeuthen/CERN group are obtained from a partly automated calculation with DIANA [16] and FORM [17, 18], using a FORTRAN code obtainable from [19]. Both codes use *LoopTools* [14].

We assume the same input values as were used in [3, 4, 5]. They are described in Tab. 1.

Fermion Masses			Boson Masses & Widths		
$m_\nu =$	0.0	GeV			
$m_e =$	0.00051099907	GeV	$m_\gamma =$	0.0	GeV
$m_\mu =$	0.105658389	GeV	$m_W =$	80.4514958	GeV
$m_\tau =$	1.77705	GeV	$m_Z =$	91.1867	GeV
$m_u =$	0.062	GeV	$m_H =$	120.0	GeV
$m_c =$	1.5	GeV	$\Gamma_W =$	0.0	GeV
$m_t =$	173.8	GeV	$\Gamma_Z =$	0.0	GeV
$m_d =$	0.083	GeV	$\Gamma_H =$	0.0	GeV
$m_s =$	0.215	GeV			
$m_b =$	4.7	GeV			
Other Parameters					
	$\alpha =$	1/137.03599976			
	$E_{\gamma_{\text{soft}}}^{\text{max}} =$	$\sqrt{s}/10$			
	$(\hbar c)^2 =$	$0.38937966 \cdot 10^9 \text{GeV}^2 \text{pb}$			

Table 1: Input parameter set.

The cross-sections shown below depend on the maximum soft-photon energy $E_{\gamma_{\text{soft}}}^{\text{max}}$. This dependence should eventually cancel when hard-photon radiation is added, but only for sufficiently small values of $E_{\gamma_{\text{soft}}}^{\text{max}}$. The value $E_{\gamma_{\text{soft}}}^{\text{max}} = \sqrt{s}/10$, which was used in the numerical evaluation, is by far too large if one aims at a high numerical accuracy after combination with real, hard-photon emission. It has been chosen here nevertheless because it ensures positive cross-section values of a realistic order of magnitude. Even for this large value, however, the numerical change in the combined soft- and hard-photon corrections compared to more realistic values of $E_{\gamma_{\text{soft}}}^{\text{max}}$ is at most few per cent at $\sqrt{s} = 500$ GeV and few per mill at $\sqrt{s} = 1$ TeV [4].

The following differential cross-sections are compared:

- $\left. \frac{d\sigma}{d\cos\theta} \right|_{\text{Born}}$: Born cross-section
- $\left. \frac{d\sigma}{d\cos\theta} \right|_{\text{B+weak}}$: Interference of Born with one-loop virtual weak corrections. The running of the electromagnetic coupling is also included in the tables²
- $\left. \frac{d\sigma}{d\cos\theta} \right|_{\text{B+w+QED+soft}}$: The QED + soft photon emission (with $E_{\gamma_{\text{soft}}}^{\text{max}} = \sqrt{s}/10$) is added to the previous contributions

The main numerical results are documented in Tabs. 2–9. Compared to [3], the agreement between our calculations for top-pair production has been improved by a factor 10^3 . This has been achieved thanks to a closer contact between both groups and a more methodological programming in the FORTRAN code TOPFIT. The agreement reaches now 11 digits of technical precision, for all flavours studied.

Finally, in Fig. 3, we give an overview of the differential cross-sections for the different flavours at two typical collider energies.

²This is not the case for the plots, where the running of the electromagnetic coupling is not included into the weak contributions.

$e^+e^- \rightarrow \tau^+\tau^- \quad \sqrt{s} = 500 \text{ GeV}$				
$\cos \theta$	$[\frac{d\sigma}{d\cos\theta}]_{\text{Born}}/\text{pb}$	$[\frac{d\sigma}{d\cos\theta}]_{\text{B+weak}}/\text{pb}$	$[\frac{d\sigma}{d\cos\theta}]_{\text{B+w+QED+soft}}/\text{pb}$	Program
-0.9	0.94591 02171 86329 $\cdot 10^{-1}$	0.10860 60371 92303	0.92419 02671 14061 $\cdot 10^{-1}$	TOPFIT
-0.9	0.94591 02171 86327 $\cdot 10^{-1}$	0.10860 60371 93233	0.92419 02671 18656 $\cdot 10^{-1}$	FA/FC
-0.5	0.89298 53117 79858 $\cdot 10^{-1}$	0.10025 68354 16001	0.86699 48248 65248 $\cdot 10^{-1}$	TOPFIT
-0.5	0.89298 53117 79856 $\cdot 10^{-1}$	0.10025 68354 16428	0.86699 48248 69477 $\cdot 10^{-1}$	FA/FC
0.0	0.15032 16827 75192	0.16418 09556 08258	0.14359 79492 08648	TOPFIT
0.0	0.15032 16827 75192	0.16418 09556 07903	0.14359 79492 08618	FA/FC
0.5	0.28649 90174 53525	0.31504 05045 07441	0.28258 86777 59811	TOPFIT
0.5	0.28649 90174 53525	0.31504 05045 06135	0.28258 86777 59161	FA/FC
0.9	0.44955 18970 14604	0.50904 21673 78790	0.47648 29191 20038	TOPFIT
0.9	0.44955 18970 14604	0.50904 21673 76612	0.47648 29191 19623	FA/FC

Table 2: Differential cross-sections for selected scattering angles for τ -production at $\sqrt{s} = 500 \text{ GeV}$. The three columns contain the Born cross-section, Born including only the weak $\mathcal{O}(\alpha)$ corrections, and Born including the weak and photonic $\mathcal{O}(\alpha)$ corrections. For each angle, the first row represents the TOPFIT result of the Zeuthen group while the second stands for the *FeynArts/FormCalc* calculation of the Munich group.

$e^+e^- \rightarrow \tau^+\tau^- \quad \sqrt{s} = 1 \text{ TeV}$				
$\cos \theta$	$[\frac{d\sigma}{d\cos\theta}]_{\text{Born}}/\text{pb}$	$[\frac{d\sigma}{d\cos\theta}]_{\text{B+weak}}/\text{pb}$	$[\frac{d\sigma}{d\cos\theta}]_{\text{B+w+QED+soft}}/\text{pb}$	Program
-0.9	0.24337 58691 13477 $\cdot 10^{-1}$	0.27641 21664 58412 $\cdot 10^{-1}$	0.23440 03881 68909 $\cdot 10^{-1}$	TOPFIT
-0.9	0.24337 58691 13477 $\cdot 10^{-1}$	0.27641 21664 60671 $\cdot 10^{-1}$	0.23440 03881 70852 $\cdot 10^{-1}$	FA/FC
-0.5	0.22648 34522 34421 $\cdot 10^{-1}$	0.25087 88401 11477 $\cdot 10^{-1}$	0.21435 50246 92009 $\cdot 10^{-1}$	TOPFIT
-0.5	0.22648 34522 34421 $\cdot 10^{-1}$	0.25087 88401 12536 $\cdot 10^{-1}$	0.21435 50246 93075 $\cdot 10^{-1}$	FA/FC
0.0	0.37338 94309 20687 $\cdot 10^{-1}$	0.40075 04507 03072 $\cdot 10^{-1}$	0.34538 81564 13972 $\cdot 10^{-1}$	TOPFIT
0.0	0.37338 94309 20687 $\cdot 10^{-1}$	0.40075 04507 02276 $\cdot 10^{-1}$	0.34538 81564 13421 $\cdot 10^{-1}$	FA/FC
0.5	0.70698 59649 23715 $\cdot 10^{-1}$	0.76863 25654 09100 $\cdot 10^{-1}$	0.68181 23407 81333 $\cdot 10^{-1}$	TOPFIT
0.5	0.70698 59649 23714 $\cdot 10^{-1}$	0.76863 25654 06057 $\cdot 10^{-1}$	0.68181 23407 78805 $\cdot 10^{-1}$	FA/FC
0.9	0.11082 80391 95421	0.12645 00486 28998	0.11773 76209 15053	TOPFIT
0.9	0.11082 80391 95421	0.12645 00486 28487	0.11773 76209 14679	FA/FC

Table 3: The same as Tab. 2 for $\sqrt{s} = 1 \text{ TeV}$.

$e^+e^- \rightarrow b\bar{b}$ $\sqrt{s} = 500$ GeV				
$\cos\theta$	$[\frac{d\sigma}{d\cos\theta}]_{\text{Born}}/\text{pb}$	$[\frac{d\sigma}{d\cos\theta}]_{\text{B+weak}}/\text{pb}$	$[\frac{d\sigma}{d\cos\theta}]_{\text{B+w+QED+soft}}/\text{pb}$	Program
-0.9	0.35947 21020 03927 $\cdot 10^{-1}$	0.42347 36269 56878 $\cdot 10^{-1}$	0.37629 38061 51582 $\cdot 10^{-1}$	TOPFIT
-0.9	0.35947 21020 03927 $\cdot 10^{-1}$	0.42347 36269 50374 $\cdot 10^{-1}$	0.37629 38061 44883 $\cdot 10^{-1}$	FA/FC
-0.5	0.52846 99142 94595 $\cdot 10^{-1}$	0.55564 40895 92051 $\cdot 10^{-1}$	0.49542 16119 64096 $\cdot 10^{-1}$	TOPFIT
-0.5	0.52846 99142 94594 $\cdot 10^{-1}$	0.55564 40895 84646 $\cdot 10^{-1}$	0.49542 16119 57136 $\cdot 10^{-1}$	FA/FC
0.0	0.13444 84372 56821	0.13513 90019 99522	0.12117 62087 02347	TOPFIT
0.0	0.13444 84372 56821	0.13513 90019 97996	0.12117 62087 00907	FA/FC
0.5	0.28324 62378 51991	0.29122 72277 53244	0.26454 12363 95596	TOPFIT
0.5	0.28324 62378 51991	0.29122 72277 50185	0.26454 12363 92671	FA/FC
0.9	0.45066 58537 60950	0.48256 44834 85869	0.44708 31668 19343	TOPFIT
0.9	0.45066 58537 60950	0.48256 44834 81057	0.44708 31668 15091	FA/FC

Table 4: The same as Tab. 2 for b -production at $\sqrt{s} = 500$ GeV.

$e^+e^- \rightarrow b\bar{b}$ $\sqrt{s} = 1$ TeV				
$\cos\theta$	$[\frac{d\sigma}{d\cos\theta}]_{\text{Born}}/\text{pb}$	$[\frac{d\sigma}{d\cos\theta}]_{\text{B+weak}}/\text{pb}$	$[\frac{d\sigma}{d\cos\theta}]_{\text{B+w+QED+soft}}/\text{pb}$	Program
-0.9	0.85256 94949 38769 $\cdot 10^{-2}$	0.98313 19956 72613 $\cdot 10^{-2}$	0.86113 09362 51944 $\cdot 10^{-2}$	TOPFIT
-0.9	0.85256 94949 38768 $\cdot 10^{-2}$	0.98313 19956 58270 $\cdot 10^{-2}$	0.86113 09362 37511 $\cdot 10^{-2}$	FA/FC
-0.5	0.12689 55586 65297 $\cdot 10^{-1}$	0.12711 32506 71243 $\cdot 10^{-1}$	0.11163 82185 03862 $\cdot 10^{-1}$	TOPFIT
-0.5	0.12689 55586 65297 $\cdot 10^{-1}$	0.12711 32506 69579 $\cdot 10^{-1}$	0.11163 82185 02235 $\cdot 10^{-1}$	FA/FC
0.0	0.32532 44660 76073 $\cdot 10^{-1}$	0.31258 65157 55267 $\cdot 10^{-1}$	0.27674 41895 03390 $\cdot 10^{-1}$	TOPFIT
0.0	0.32532 44660 76072 $\cdot 10^{-1}$	0.31258 65157 51750 $\cdot 10^{-1}$	0.27674 41894 99947 $\cdot 10^{-1}$	FA/FC
0.5	0.68639 85356 49626 $\cdot 10^{-1}$	0.69302 03325 89997 $\cdot 10^{-1}$	0.62501 12097 14961 $\cdot 10^{-1}$	TOPFIT
0.5	0.68639 85356 49626 $\cdot 10^{-1}$	0.69302 03325 82884 $\cdot 10^{-1}$	0.62501 12097 07973 $\cdot 10^{-1}$	FA/FC
0.9	0.10923 62308 06567	0.12127 77274 48650	0.11240 86957 39236	TOPFIT
0.9	0.10923 62308 06567	0.12127 77274 47528	0.11240 86957 38153	FA/FC

Table 5: The same as Tab. 2 for b -production at $\sqrt{s} = 1$ TeV.

$e^+e^- \rightarrow c\bar{c} \quad \sqrt{s} = 500 \text{ GeV}$				
$\cos \theta$	$[\frac{d\sigma}{d\cos\theta}]_{\text{Born}} / \text{pb}$	$[\frac{d\sigma}{d\cos\theta}]_{\text{B+weak}} / \text{pb}$	$[\frac{d\sigma}{d\cos\theta}]_{\text{B+w+QED+soft}} / \text{pb}$	Program
-0.9	0.78403 69156 96992 $\cdot 10^{-1}$	0.91244 84607 87569 $\cdot 10^{-1}$	0.83668 39315 90920 $\cdot 10^{-1}$	TOPFIT
-0.9	0.78403 69156 96992 $\cdot 10^{-1}$	0.91244 84607 99371 $\cdot 10^{-1}$	0.83668 39316 04269 $\cdot 10^{-1}$	FA/FC
-0.5	0.10411 12875 82399	0.11650 15689 39071	0.10590 20427 16561	TOPFIT
-0.5	0.10411 12875 82399	0.11650 15689 39412	0.10590 20427 16692	FA/FC
0.0	0.24770 82888 4590 1	0.26255 80017 68786	0.23448 15990 25778	TOPFIT
0.0	0.24770 82888 4590 0	0.26255 80017 67528	0.23448 15990 23961	FA/FC
0.5	0.51515 25192 73431	0.53094 95526 19036	0.46371 41775 17198	TOPFIT
0.5	0.51515 25192 73431	0.53094 95526 15566	0.46371 41775 12847	FA/FC
0.9	0.81827 79086 1355 7	0.83043 43356 61887	0.70026 97050 29472	TOPFIT
0.9	0.81827 79086 1355 6	0.83043 43356 56199	0.70026 97050 21870	FA/FC

Table 6: The same as Tab. 2 for c -production at $\sqrt{s} = 500 \text{ GeV}$.

$e^+e^- \rightarrow c\bar{c} \quad \sqrt{s} = 1 \text{ TeV}$				
$\cos \theta$	$[\frac{d\sigma}{d\cos\theta}]_{\text{Born}} / \text{pb}$	$[\frac{d\sigma}{d\cos\theta}]_{\text{B+weak}} / \text{pb}$	$[\frac{d\sigma}{d\cos\theta}]_{\text{B+w+QED+soft}} / \text{pb}$	Program
-0.9	0.20476 82671 10479 $\cdot 10^{-1}$	0.23804 15350 74367 $\cdot 10^{-1}$	0.21460 20354 03294 $\cdot 10^{-1}$	TOPFIT
-0.9	0.20476 82671 10479 $\cdot 10^{-1}$	0.23804 15350 77280 $\cdot 10^{-1}$	0.21460 20354 06337 $\cdot 10^{-1}$	FA/FC
-0.5	0.26302 86046 48394 $\cdot 10^{-1}$	0.29192 27449 28377 $\cdot 10^{-1}$	0.26283 52825 19898 $\cdot 10^{-1}$	TOPFIT
-0.5	0.26302 86046 48394 $\cdot 10^{-1}$	0.29192 27449 29292 $\cdot 10^{-1}$	0.26283 52825 20679 $\cdot 10^{-1}$	FA/FC
0.0	0.61063 66375 8392 1 $\cdot 10^{-1}$	0.63092 30352 27478 $\cdot 10^{-1}$	0.55698 44755 91055 $\cdot 10^{-1}$	TOPFIT
0.0	0.61063 66375 8392 0 $\cdot 10^{-1}$	0.63092 30352 24633 $\cdot 10^{-1}$	0.55698 44755 87819 $\cdot 10^{-1}$	FA/FC
0.5	0.12635 58682 75626	0.12548 22393 89320	0.10778 82066 27453	TOPFIT
0.5	0.12635 58682 75626	0.12548 22393 88519	0.10778 82066 26582	FA/FC
0.9	0.20057 22407 70464	0.19463 36446 48183	0.16019 87823 32139	TOPFIT
0.9	0.20057 22407 70464	0.19463 36446 46866	0.16019 87823 30647	FA/FC

Table 7: The same as Tab. 2 for c -production at $\sqrt{s} = 1 \text{ TeV}$.

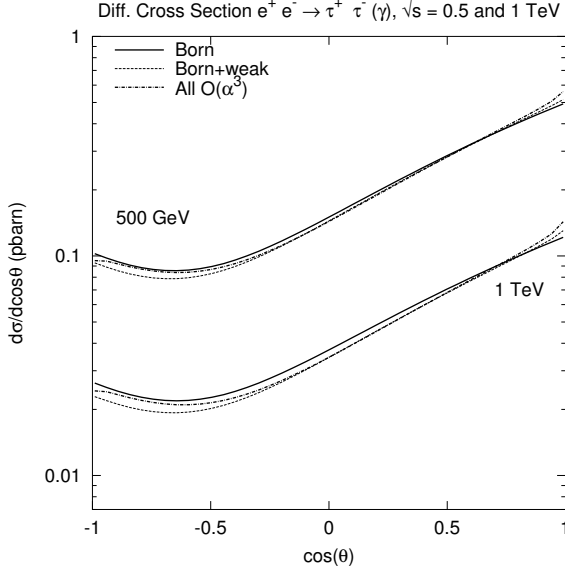
$e^+e^- \rightarrow t\bar{t} \quad \sqrt{s} = 500 \text{ GeV}$				
$\cos \theta$	$[\frac{d\sigma}{d\cos\theta}]_{\text{Born}}/\text{pb}$	$[\frac{d\sigma}{d\cos\theta}]_{\text{B+weak}}/\text{pb}$	$[\frac{d\sigma}{d\cos\theta}]_{\text{B+w+QED+soft}}/\text{pb}$	Program
-0.9	0.10883 91940 76039	0.12425 90371 32943	0.11408 40955 77861	TOPFIT
-0.9	0.10883 91940 76039	0.12425 90371 33664	0.11408 40955 78964	FA/FC
-0.5	0.14227 50693 93371	0.15684 83718 76069	0.14308 12051 65511	TOPFIT
-0.5	0.14227 50693 93371	0.15684 83718 76250	0.14308 12051 65581	FA/FC
0.0	0.22547 04640 33559	0.24026 68040 30724	0.21718 80097 67412	TOPFIT
0.0	0.22547 04640 33559	0.24026 68040 30032	0.21718 80097 66323	FA/FC
0.5	0.35466 64703 33217	0.36888 65069 94389	0.32933 72739 51692	TOPFIT
0.5	0.35466 64703 33217	0.36888 65069 92599	0.32933 72739 49095	FA/FC
0.9	0.49114 37157 67761	0.50333 75116 05520	0.44290 81673 51494	TOPFIT
0.9	0.49114 37157 67761	0.50333 75116 02681	0.44290 81673 46094	FA/FC

Table 8: The same as Tab. 2 for t -production at $\sqrt{s} = 500 \text{ GeV}$.

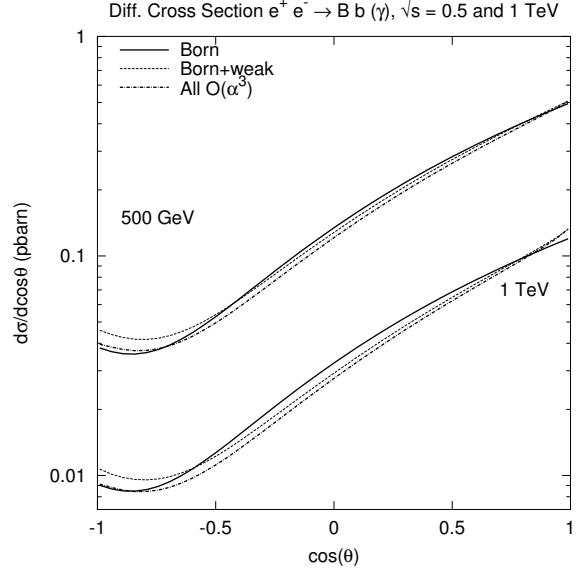
$e^+e^- \rightarrow t\bar{t} \quad \sqrt{s} = 1 \text{ TeV}$				
$\cos \theta$	$[\frac{d\sigma}{d\cos\theta}]_{\text{Born}}/\text{pb}$	$[\frac{d\sigma}{d\cos\theta}]_{\text{B+weak}}/\text{pb}$	$[\frac{d\sigma}{d\cos\theta}]_{\text{B+w+QED+soft}}/\text{pb}$	Program
-0.9	0.22785 42327 32090 $\cdot 10^{-1}$	0.25521 28532 98051 $\cdot 10^{-1}$	0.23101 70508 05040 $\cdot 10^{-1}$	TOPFIT
-0.9	0.22785 42327 32090 $\cdot 10^{-1}$	0.25521 28533 00748 $\cdot 10^{-1}$	0.23101 70508 07714 $\cdot 10^{-1}$	FA/FC
-0.5	0.29782 13110 31861 $\cdot 10^{-1}$	0.31863 48943 59857 $\cdot 10^{-1}$	0.28823 01902 00931 $\cdot 10^{-1}$	TOPFIT
-0.5	0.29782 13110 31861 $\cdot 10^{-1}$	0.31863 48943 60711 $\cdot 10^{-1}$	0.28823 01902 01653 $\cdot 10^{-1}$	FA/FC
0.0	0.61180 06742 25039 $\cdot 10^{-1}$	0.61591 61295 77963 $\cdot 10^{-1}$	0.54950 88904 88739 $\cdot 10^{-1}$	TOPFIT
0.0	0.61180 06742 25038 $\cdot 10^{-1}$	0.61591 61295 75474 $\cdot 10^{-1}$	0.54950 88904 85894 $\cdot 10^{-1}$	FA/FC
0.5	0.11774 69498 88318	0.11404 76860 51226	0.99417 00898 39905 $\cdot 10^{-1}$	TOPFIT
0.5	0.11774 69498 88318	0.11404 76860 50527	0.99417 00898 32292 $\cdot 10^{-1}$	FA/FC
0.9	0.18112 20970 86446	0.17134 61927 22790	0.14426 23325 41248	TOPFIT
0.9	0.18112 20970 86446	0.17134 61927 21645	0.14426 23325 40061	FA/FC

Table 9: The same as Tab. 2 for t -production at $\sqrt{s} = 1 \text{ TeV}$.

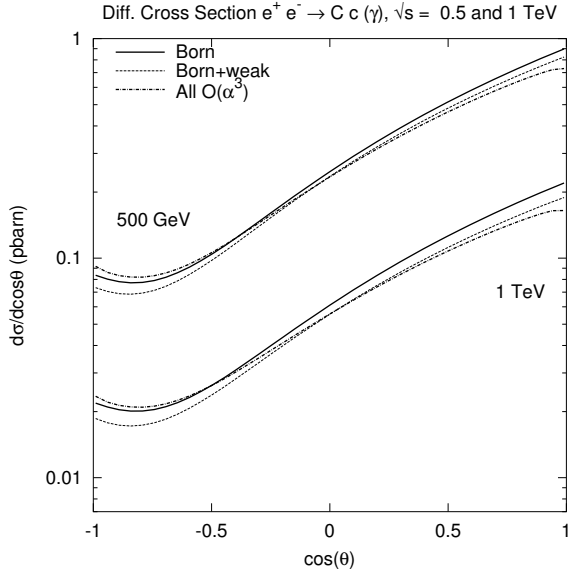
a) τ production.



b) b production.



c) c production.



d) t production.

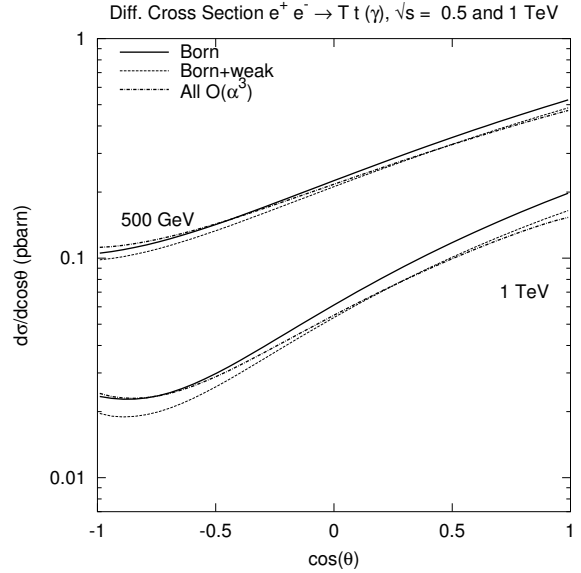


Figure 3: Comparison of differential cross-sections. Solid line stands for Born, dashed for Born+weak (without running coupling), and dashed-dotted for complete $\mathcal{O}(\alpha)$ (i.e. Born+weak+QED+soft).

References

- [1] ECFA/DESY LC Physics Working Group (J. Aguilar-Saavedra et al.), “TESLA Technical Design Report Part III: Physics at an e^+e^- Linear Collider,” DESY 2001–011 (2001), [hep-ph/0106315](#).
- [2] G. Passarino and M. Veltman, *Nucl. Phys.* **B160** (1979) 151.
- [3] J. Fleischer, T. Hahn, W. Hollik, T. Riemann, C. Schappacher, and A. Werthenbach, “Complete electroweak one-loop radiative corrections to top-pair production at TESLA: A comparison,” preprint LC-TH-2002-002 (2002), [hep-ph/0202109](#).
- [4] J. Fleischer, J. Fujimoto, T. Ishikawa, A. Leike, T. Riemann, Y. Shimizu, and A. Werthenbach, “One-loop corrections to the process $e^+e^- \rightarrow t\bar{t}$ including hard bremsstrahlung,” in *Second Symposium on Computational Particle Physics (CPP, Tokyo, 28–30 Nov 2001)*, KEK Proceedings 2002-11 (2002) (Y. Kurihara, ed.), pp. 153–162, [hep-ph/0203220](#).
- [5] J. Fleischer, A. Leike, T. Riemann, and A. Werthenbach, [hep-ph/0302259](#), to appear in *Eur. Phys. J. C*.
- [6] K. Kolodziej, *Eur. Phys. J.* **C23** (2002) 471–477, [hep-ph/0110063](#);
- [7] S. Dittmaier and M. Roth, *Nucl. Phys.* **B642** (2002) 307–343, [hep-ph/0206070](#);
- [8] S. Dittmaier and M. Roth, *Nucl. Phys. Proc. Suppl.* **116** (2003) 38–42, [hep-ph/0210168](#).
- [9] E. Accomando *et al.*, “Standard model processes,” in *Physics at LEP2*, report CERN 96–01 (1996) (G. Altarelli, T. Sjöstrand, and F. Zwirner, eds.), pp. 207–248, 1996, [hep-ph/9601224](#).
- [10] Two Fermion Working Group (M. Kobel et al.), “Two-fermion production in electron positron collisions,” in *Reports of the working groups on precision calculations for LEP2 physics*, Proc. of the Monte Carlo Workshop, Geneva, 1999-2000, report CERN 2000-09-D (2000) (S. Jadach, G. Passarino, and R. Pittau, eds.), pp. 269–378, [hep-ph/0007180](#).
- [11] W. Beenakker, S. van der Marck, and W. Hollik, *Nucl. Phys.* **B365** (1991) 24–78.
- [12] J. Küblbeck, M. Böhm, and A. Denner, *Comput. Phys. Commun.* **60** (1990) 165–180.
- [13] T. Hahn, *Comput. Phys. Commun.* **140** (2001) 418–431, [hep-ph/0012260](#).
- [14] T. Hahn and M. Perez-Victoria, *Comput. Phys. Commun.* **118** (1999) 153–165, [hep-ph/9807565](#).
- [15] T. Hahn, *Nucl. Phys. Proc. Suppl.* **116** (2003) 363, [hep-ph/0210220](#).

- [16] M. Tentyukov and J. Fleischer, *Comput. Phys. Commun.* **132** (2000) 124–141, [hep-ph/9904258](#).
- [17] J. Vermaseren, “Symbolic manipulation with FORM” (Computer Algebra Nederland, Amsterdam, 1991);
- [18] J. Vermaseren, “New features of FORM”, [math-ph/0010025](#).
- [19] J. Fleischer, A. Leike, A. Lorca, T. Riemann, and A. Werthenbach, Fortran program TOPFIT v.0.92 (01 July 2003), <http://www-zeuthen.desy.de/~riemann/>.